eTransportation 8 (2021) 100102

Contents lists available at ScienceDirect

eTransportation

journal homepage: www.journals.elsevier.com/etransportation

Evolution of initial cell-to-cell variations during a three-year production cycle

M. Schindler *, J. Sturm , S. Ludwig , J. Schmitt , A. Jossen

Institute for Electrical Energy Storage Technology, Technical University of Munich (TUM), Arcisstr. 21, 80333, Munich, Germany

ARTICLE INFO

Article history:
Received 23 July 2020
Received in revised form
18 November 2020
Accepted 23 December 2020
Available online 1 January 2021

Keywords:
Lithium-ion battery
Cell-to-cell variation
Manufacturing quality
Differential voltage analysis
Cell matching

ABSTRACT

Consistent quality of the battery system in battery electric vehicles (BEVs) is highly dependent on constant quality of the supplied individual cells. Especially for promising, relatively novel material combinations, cell-to-cell parameter variations may vary over years, since cell manufacturers might have not yet found the ideal composite to produce cells with high capacity and cycle stability. This study investigates the development of cells' capacity, internal resistance and energy density over a time span of nearly three years for three different batches of the same cell. The cell under investigation is commercially available and offers a promising material combination of silicon-graphite and nickel-rich NMC. Differential voltage and differential capacity analysis are used to explain possible reasons for cell-to-cell variations. As a result, we found significant differences in cell-to-cell variations between the batches. For BEV manufacturers, this means in particular that they should consider how they can counter the influence of these cell-to-cell variations through an operating strategy in order to protect themselves in the long term against regress claims by customers.

1. Introduction

For manufacturers of battery modules and packs, the analysis of cell-to-cell variations is increasingly becoming a key feature to guarantee the efficiency of their battery modules and packs over a lifetime by evaluating and matching the physical properties of single cells to ensure consistency across the module. The aim of these analyses is to quantify the variance of the cells' capacity (C), the internal resistance (R_i) and the open-circuit-voltage (OCV) characteristics of the investigated lithium-ion batteries (LIBs) [1]. As a result, battery module and pack manufacturers can reconsider their so-called cell-matching strategies [2] with our findings in terms of long-term cell manufacturing variance.

Since the typical production period of vehicle models covers several years, the cell-to-cell variations can change significantly during this period due to modified or optimized cell production processes. In this context, experimental data are often unavailable and assumptions about the impact of cell manufacturing variance are based on values from the literature [3]. In particular studies on possible changes in cell property variance during a long term production cycle have not yet been presented in the literature. This work may help to fill in this gap by presenting cell-to-cell variations for three different batches over a time span of almost three years.

Cell-to-cell variations often fit a normal distribution [4]. In this work, the mean values μ_C and μ_R of the measured C and R_i are evaluated together with their standard deviations σ_C and σ_R. The smaller the values for σ_C and σ_R, the smaller the dispersion of the analyzed batch. We apply relative coefficients of variation κ_C and κ_R, which represent the percentage by which the standard deviation varies with respect to the mean value, $\kappa = \sigma/\mu$. If one aims to compare different studies, κ_C and κ_R can be seen as the important parameters to compare different data sets [5]. However, only a few publications provide sufficient statistical information about relevant cell-to-cell variations to determine these values. Table 1 gives an overview of the present analysis in the literature. Investigations based on simulation (Refs. [6,7]) have to be differentiated from measurement studies. As the presented results are based on measurement data, studies based on simulation data are listed in order to preserve integrity but will not be discussed further.

As indicated within Table 1, different measurement techniques can be used to determine the cells' capacities and internal resistances. Generally, capacity measurement can be done using either constant current (CC) [8–11,15–19] or constant current - constant voltage (CC-CV) [1,5,12,13] measurement. Furthermore,

* Corresponding author.
E-mail address: markus.ms.schindler@tum.de (M. Schindler).

https://doi.org/10.1016/j.etran.2020.100102

Table 1
Overview of the latest studies from literature analyzing cell-to-cell variations of capacity and impedance behavior of LIBs.

Reference	Sample Size	Chemistry	μ_C in Ah	κ_C in %	μ_R in mΩ	κ_R in %	Factor κ_R/κ_C
Shin* [6]	10,000	–	0.29	2.9	0.28[c]	4.4	1.5
Paul* [7]	20,000	C/LFP[I,II]	4.40	1.3	–	5.8	4.5
Rumpf [1]	600	C/LFP	3.02[a]	0.2	17.6[d]	1.8	7.7
Rumpf [1]	500	C/LFP	3.03[a]	0.3	17.7[d]	0.7	2.1
Zheng [8]	96	C/LFP	>70[b]	–	0.53[d]	19.5	–
Dubarry [9]	100	C/LCO[III]	0.30[b]	1.9	–	–	–
Devie [10]	51	C/LCO-NMC[IV]	2.86[b]	0.4	73.2[e]	3.6	9.0
Dubarry [11]	10	C/LCO-LMO[V]	1.89[b]	0.2	67.1[e]	5.7	36
Campestrini [12]	250	C/NCA[VI]	2.88[a]	0.2	21.7[f]	0.7	4.5
Baumann [13]	164	C/NCA	2.88[a]	0.4	36.0[e]	0.9	2.6
An [14]	5,473**	C/NCA-NMC	5.41[b]	0.5	–	–	–
An [15]	7739	C/NMC	–	–	–	–	–
Rothgang [16]	700	C/NMC	5.06[b]	2.4	3.0[e]	2.9	1.2
Schuster [5]	484	C/NMC	1.97[a]	0.8	71.2[d]	1.9	2.4
Barreras [17]	>200	C/NMC	51.8[a]	0.3	1.42[e]	5.6	18.7
Baumhöfer [18]	48	C/NMC	1.85[a]	0.5	–	–	–
Zou [19]	248	–	3.01[b]	0.4	13.8[c]	1.0	2.6

* Results are based on simulation data. ** Only 198 cells were evaluated for μ_C and κ_C
[I] Graphite (C). [II] Lithium Iron Phosphate (LFP). [III] Lithium Cobalt Oxide (LCO)
[IV] Nickel Manganese Cobalt oxide (NMC). [V] Lithium Manganese Oxide (LMO). [VI] Nickel Cobalt Aluminum oxide (NCA)
[a] CC-CV discharge capacity. [b] CC discharge capacity. [c] No information on the measurement procedure available
[d] EIS (Im(Z) = 0). [e] DC pulse. [f] AC (1 kHz)

either charging, discharging or charging-discharging capacities can be evaluated. On the other hand, direct current (DC) pulses [10,11,13,16,17], alternating current (AC) measurement at 1 kHz ([12]) or electrochemical impedance spectroscopy (EIS) [1,5,8] are normally used to determine the internal resistance of the cell [13].

For the determination of the cell capacity, the measuring method and C-rate applied have an impact, as does whether the measurement is conducted in the charging or discharging direction. Within Table 1, the cells' capacity was defined mainly by the CC discharge capacity for a defined C-rate of 0.2C [10,15,19], 0.3C [8], 0.5C [9,11] or 1C [16–18], except for [18] which evaluated the 1C CC charging capacity. The CC-CV capacities were always measured using a 1C discharge rate and a cut-off current amplitude of 0.05C [1,5,12,13]. Since there is no standard method in the literature to determine the cell capacity, cell capacity in this study refers to the CC-CV discharge capacity unless otherwise specified.

For the evaluation of the internal resistance via DC pulses, the pulse duration has a major influence on the result. It can be assumed that as the pulse duration increases, the measured result for R_i also includes other resistance fractions, such as the diffusion polarization resistance in addition to the purely ohmic resistance [1,16,20]. Measurement results that are based on a pulse duration of several seconds [13,16,20], can therefore only be compared to a limited extent with results obtained by evaluating the voltage response recorded up to 1 s after the current pulse [10,11,17,20]. On the other hand, EIS measurement results depicted from the zero crossing of Im(Z) [1,5,8] correlate highly with the determined values at 1 kHz [12] which is why these measurement techniques can be seen as equivalent and well comparable [1]. Therefore, EIS measurement evaluated at Im(Z) is used to evaluate the cells internal resistances within this study.

Nevertheless, in order to be able to compare different studies, the values for κ_C and κ_R can be used according to Rumpf et al. [1]. If in the literature the necessary values for μ and σ of C and R_i were given to calculate κ_C and κ_R, it turns out that there are always lower values for κ_C compared to κ_R (see Table 1). According to An et al. [15], this result is expected because C is the most commonly used characteristic by cell manufacturers for a LIB, normally used as the decisive criterion for cell matching. In general, κ_C and κ_R are within the range of 0.2% to 2.4% and 0.7% to 5.7% respectively. The relative coefficient κ_R of Zheng et al. [8] (19.5%) appears relatively high and can be seen as an outlier. The exact reasons could not be determined due to the data provided by Zheng et al. [8]. Additionally, it is worth highlighting that except from Ref. [8] ($\mu_C > 70$ Ah) and [17] ($\mu_C = 51.8$ Ah), only cells with a maximum capacity around 5.5 Ah are analyzed within the literature. A possible reason for this phenomenon is that large format cells are more cost intensive and additionally, the required measurement equipment might not be available.

As illustrated by Table 1, the cells examined in the literature show a variety of analyzed material combinations on the cathode side, ranging from LFP, LCO, NCA and NMC-111 to blends like LCO-NMC, LCO-LMO or NCA-NMC. However, current trends for the cathode incorporated especially nickel-rich types such as NMC-811 (nickel-rich NMC) or NCA. In order to compensate for the gravimetric capacity on the anode side, silicon is often added to the graphite electrode [11,21]. Consequently, investigations of cell-to-cell variations for material combinations of silicon-graphite SiC/NMC-811 are of particular interest but currently missing in the literature. Furthermore, none of these investigations has so far accompanied the same cell type in a long-term manner, and analysis of possible changes of C and R_i are neither present nor their causes explained. Therefore, this paper aims to close this gap by presenting cell-to-cell variations for three batches of a commercially available 18650 cell (SiC/NMC-811), bought over a period of almost three years. Additionally, differential voltage analysis (DVA) and differential capacity analysis (DCA) as well as an energy density metric are used to investigate the reasons for the development of C and R_i during this section of the product life cycle.

2. Experimental

The cell under investigation has a nominal capacity of 3.35 Ah and has the form factor 18650. The anode material consists of SiC and the cathode material is based on nickel-rich NMC-811. Over a period of almost three years, three different orders with different cell quantities were taken from a commercial supplier. The first order included 48 cells (Batch 1, B_1), the second 160 (Batch 2, B_2) and the third 200 cells (Batch 3, B_3). Consequently, a total of 408 cells were examined. Every order requested cells of the same production batch to ensure that all cells within a batch were manufactured under equal conditions. Requests for modified cell compositions as compared to former orders were denied by the supplier. Within a batch, cells were signed with a production code allowing the determination of production dates of different batches. Table 2 summarizes the information of the investigated batches.

Since measurement equipment and climate chambers are limited, the cells were stored at the delivery status without any charging or discharging at 5 °C and 30% state of charge (SOC) to reduce side reactions and improve comparability. Subsequently, the measurement was performed within climate chambers (KT115, Binder) at 25 °C using terminal boards, including gold-plated spring contact pins and four-wire configuration (F840, Feinmetall). A cycler (CTS, BaSyTec) and a potentiostat (VMP3, BioLogic) were used to apply the steps summarized in Table 3 and described in the following. As the cells were stored at 5 °C, an initial resting time of 6 h was applied to ensure sufficient time to reach a homogeneous cell temperature of 25 °C (step 1) before performing measurements. Initially, 2 full cycles (FC) including CC and constant voltage (CV) charge (Ch) and discharge (Dch) phases were performed to reactivate the cells' kinetics (step 2). Additionally, 5 conditioning FC without CV phases were performed to create equal initial conditions (step 3) and reduce deviations within the formation of the cells without possibly damaging the cells by extensive CV phases. Dubarry et al. [11] showed that applying initial conditioning leads to a similar initial reference state for all cells, and reduces possible remaining variances evoked by the manufacturer's formation and the different storage periods afterward. With reference to the examined cells, it should be noted that according to the data sheet, a higher loss of capacity per cycle is to be expected during the first cycles. As Table A.6 shows, the difference between the capacity loss per cycle decreases during the conditioning cycles from values above 12 mAh to values under 1.5 mAh. Therefore, it can be assumed that the conditioning cycles contribute to improving the consistency of the measurement of the CC-CV discharge capacity, which is evaluated during the second FC of step 4 of the test sequence.

Subsequently, the parameter R_i was determined at a SOC of 50% using galvanostatic EIS (step 5). The measurement was performed within the frequency range of 10 mHz to 10 kHz with a current amplitude of 140 mA. Finally, R_i was evaluated at $\mathrm{Im}(Z) = 0$, the zero crossing of the imaginary part. Fig. A.7 illustrates the measured EIS curves for a representative cell of each analyzed batch.

Within all cycles, the cell voltage limits were set to 4.2 V and 2.5 V, as recommended by the manufacturer. The applied charge $I_{\mathrm{Ch\text{-}CC}}$ and discharge $I_{\mathrm{Dch\text{-}CC}}$ currents as well as the cut-off current of 50 mA during CV charging $I_{\mathrm{Ch\text{-}CV}}$ were selected according to the data sheet of the cells. The cut-off criteria during CV discharging $I_{\mathrm{Dch\text{-}CV}}$ was accordingly based on $I_{\mathrm{Ch\text{-}CV}}$. The number of cycles for activation and capacity check were adopted from previous studies [1,22]. The number of conditioning cycles is based on the findings of [11], who showed that typically 3–6 conditioning cycles are sufficient to stabilize the capacity of the cells between two consecutive cycles.

Finally, the OCV was measured (step 6) to perform the DVA and DCA of the cells (discharge direction) in the following. Table 3 summarizes the test procedure, including current amplitudes and cut-off criteria. The same procedure was also used in former studies by Zilberman et al. [22].

The total test time of the test procedure shown in Table 3 is approximately 8.5 days, including pauses. The total test time appears to be relatively long as compared to only the capacity check (approximately 1 day). However, the test time can be justified, since in addition to activation and conditioning cycles to improve results, EIS and OCV measurements are also performed for subsequent in-depth investigations. If OCV measurement is not required and R_i is determined by step response, the total test time could be reduced to approximately 4.5 days.

Besides the duration of the test sequence, the required total test time also depends on the number of cells and the available test capacity. It was possible to test an average 25 cells at once for B_1; for B_2 and B_3 it was possible to test an average of 40 cells at once. Therefore, the total test time required for B_1 was approximately 17 days, for B_2 approximately 34 days and for B_3 approximately 42 days. If less testing capacity is available the test time per cell can be reduced by adjusting the time for thermal conditioning and the duration of the pauses. In this study, the chosen times were based on empirical values, where it could be assured that the times were sufficient to achieve a homogeneous temperature distribution within the cell and to ensure that subsequent tests were not influenced by previous ones.

Before discussing the results of this study, possible influences of the anode overhang on the measurement results should be discussed. Gyenes et al. described the influence of the anode overhang on coulombic efficiency and capacity measurements in Ref. [23]. Within their experiment, cells were stored for 100 h at varying SOCs before the charge and discharge capacity was evaluated after different time spans. As a result, a difference of nearly 2 mAh (discharge capacity) would be expected between the first measurement after storage (approx. 25 h) and after 800 h (approx. 33 days) for cells stored at 20% SOC. With respect to the present study, the longest time span between delivery and start of the last test run was approx. 32 days (768 h) for B_3. Assuming, that the same results apply to cells stored at 30% SOC, a difference of 2 mAh to the average capacity of B_3 (see Table 4) would provoke a maximum deviation of 0.06%. Since this deviation appears relatively low, no influence of the anode overhang on the results are assumed, which is why the influence of the anode overhang will not be discussed further in the following.

Table 2
Summary of production date, delivery date and quantities of the investigated batches.

	Production	Delivery	Quantity
B_1	09.2016	01.2017	48
B_2	10.2017	03.2018	160
B_3	12.2018	05.2019	200

3. Results

The distribution of the CC-CV discharge capacity of batches 1–3 is illustrated in Fig. 1. The distributions seem to deviate from the assumed normal distribution. Nevertheless, the calculation of μ and σ are applied to the different batches, as this was the case within the studies of [1,7] for equally deviating distributions. The mean capacities μ_{C1}, μ_{C2} and μ_{C3} of the batches amount to 3.49 Ah, 3.43 Ah and 3.38 Ah. Since normal distribution is assumed for the capacity, the standard deviations σ_{C1}, σ_{C2} and σ_{C3} amount to 7.1 mAh, 12.4 mAh and 13.4 mAh. Furthermore, the relative coefficients of variation κ_{C1}, κ_{C2}, κ_{C3} of the capacity, representing the ratio of σ_C and μ_C amount to 0.2%, 0.4% and 0.4% for the different batches.

Fig. 2 illustrates the results of R_i of the cells, calculated from the EIS measurement results. The mean internal resistances μ_{R1}, μ_{R2} and μ_{R3} of the batches amount to 30.8 mΩ, 28,7 mΩ and 29.4 mΩ. Furthermore, the values of σ_{R1}, σ_{R2} and σ_{R3} amount to 0.2 mΩ, 0.3 mΩ and 1.0 mΩ. Additionally, the relative coefficients of variation κ_{R1}, κ_{R2} and κ_{R3} of the internal resistance κ_R, representing the ratio of σ_R and μ_R amount to 0.7%, 0.9% and 3.4% for the different batches.

The energy density distribution for batches 1–3 is illustrated in Fig. 3. The mean energy densities $\mu_{\omega 1}$, $\mu_{\omega 2}$ and $\mu_{\omega 3}$ of the batches are 274 Wh kg^{-1}, 268 Wh kg^{-1} and 265 Wh kg^{-1}. Note, that at the time of producing the data to calculate the energy density, only 127 cells of B_2 and 178 cells of B_3 were available. However, despite the missing number of cells, it can be assumed that the overall result is not affected by this. Table 4 summarizes the results of the investigated cell-to-cell variations.

Fig. 4 illustrates the results of the mean DVA for B_1, B_2 and B_3. The complete measurement data of the DVA is illustrated in Fig. A.6 a). Zilberman et al. [21] introduced distinctive DVA markers to quantify

Table 3
Sequence of the tests performed to investigate cell-to-cell variations. C was determined in step 4 by the sum of CC and CV discharge capacity. R_i was determined by an EIS at 50% SOC (Im(Z) = 0). Cells were cycled between 4.2 V and 2.5 V. $I_{Ch\text{-}CV}$ and $I_{Dch\text{-}CV}$ represent the absolute cell current limits of the corresponding CV phase. All tests were performed at an ambient temperature of 25 °C.

Step	Sequence	Duration	$I_{Ch\text{-}CC}$	$I_{Ch\text{-}CV}$	$I_{Dch\text{-}CC}$	$I_{Dch\text{-}CV}$	$t_{Ch\text{-}Dch}$	N_{FC}
1	Thermal Conditioning	6 h	–	–	–	–	–	–
2	Activation	–	0.5 C	50 mA	0.2 C	50 mA	0.5 h	2
	Pause	6 h	–	–	–	–	–	–
3	Conditioning Cycles	–	0.5 C	–	0.2 C	–	0.5 h	5
	Pause	6 h	–	–	–	–	–	–
4	Capacity Check	–	0.5 C	50 mA	0.2 C	50 mA	0.5 h	2
	Pause	6 h	–	–	–	–	–	–
5	EIS[a]	–	–	–	–	–	–	–
6	OCV	–	0.03 C	3.5 mA	0.03 C	3.5 mA	6 h	1

[a] $f \in [10\,\text{mHz}; 10\,\text{kHz}]$, $\hat{I} = 140$ mA, 13/10/5 points per decade within [10 kHz; 1 Hz]/[1 Hz; 100 mHz]/[100 mHz; 10 mHz].

Table 4
Summary of cell-to-cell variations of the investigated batches.

Batch	Quantity	μ_C	σ_C	κ_C	μ_R	σ_R	κ_R	μ_ω
B_1	48	3.49 Ah	7.1 mAh	0.2%	30.8 mΩ	0.2 mΩ	0.7%	274 Wh kg^{-1}
B_2	160	3.43 Ah	12.4 mAh	0.4%	28.9 mΩ	0.3 mΩ	0.9%	268 Wh kg^{-1}
B_3	200	3.38 Ah	13.4 mAh	0.4%	29.4 mΩ	1.0 mΩ	3.4%	265 Wh kg^{-1}

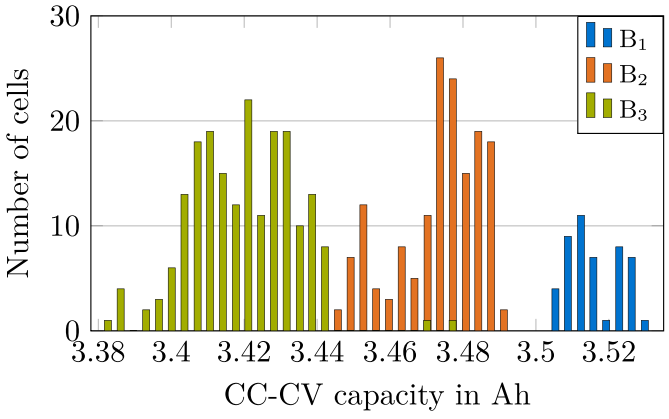

Fig. 1. Distribution of the CC-CV capacity of the different batches. The mean capacity decreased continuously from 3.49 Ah to 3.43 Ah and 3.38 Ah (B_1 to B_3).

characteristic values for the capacities of active electrode components. Generally, the markers can be assigned to capacities of different material components of the cell, namely silicon (Si), C, SiC, NMC and SiC/NMC. In order to describe the differences of the analyzed batches, the assignment of these capacities to specific DVA peaks as well as a quantification of the capacities is described in the following. The values of $Q_{Si,I}$ and $Q_{Si,II}$ can be assigned to the first and second peak occurring between 0% and approx. 15% SOC. For both capacities, it can be stated that B_1 has the highest capacity, followed by B_2 and B_3 ($B_1 > B_2 > B_3$). The same applies to Q_{SiC}, which is characterized by the area between the left border of the DVA and the main graphite peak around 60% SOC. The capacities of $Q_{C,I-III}$, are represented by the peaks within the range of 20% to 40% and the main graphite peak. For these capacities, a clear order of the batches cannot be given (see Table 5). The capacity of Q_{NMC} is described by the range between the peak next to 80% SOC and the minimum next to 90% SOC. Here, $B_1 < B_2 < B_3$ accounts for the capacities of the different batches. Finally, the values of the capacity of $Q_{NMC/SiC}$ are again in the $B_1 > B_2 > B_3$ order. $Q_{NMC/SiC}$ is represented by the area between the peak next to 80% SOC and the right border of the DVA curve. Table 5 summarizes the quantitative order of the batches for the different capacities and their percentage deviation from B_1. Consequently, anode- and cathode-specific capacities containing Si show a greater deviation as compared to capacities referring only to the pure C and NMC-811.

According to Jung et al. [24] and Fuchsbichler et al. [25], the peaks of the averaged DCAs illustrated in Fig. 5 can be assigned as follows:

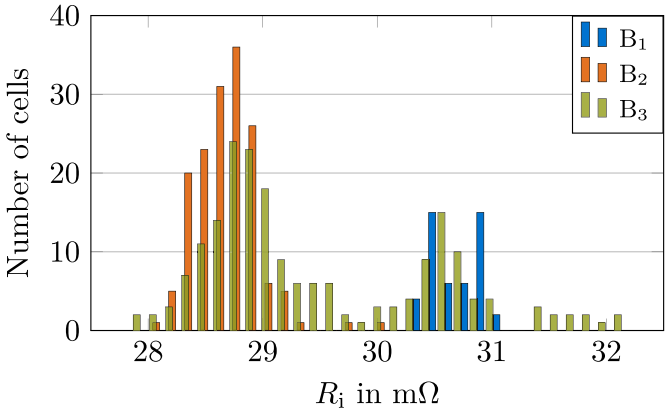

Fig. 2. Results of the EIS measurement performed for the variation of the impedance behavior (R_i). The mean values of R_i of B_2 and B_3 (28.69 mΩ and 29.35 mΩ) are decreased as compared to 30.78 mΩ of B_1.

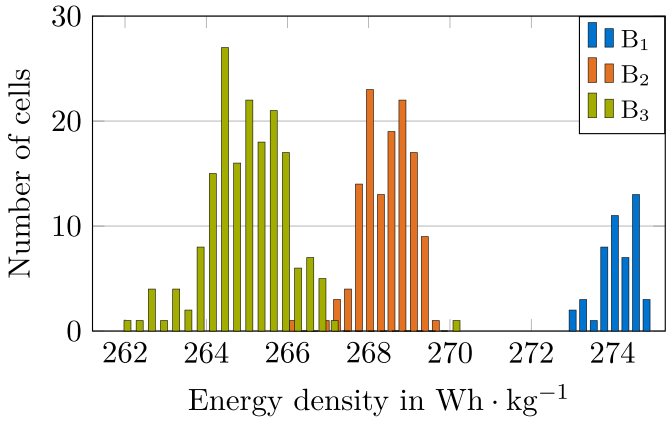

Fig. 3. Distribution of the energy density of the different batches. The mean energy density decreased continuously from 274 Wh kg^{-1} to 268 Wh kg^{-1} and 265 Wh kg^{-1} (B_1 to B_3).

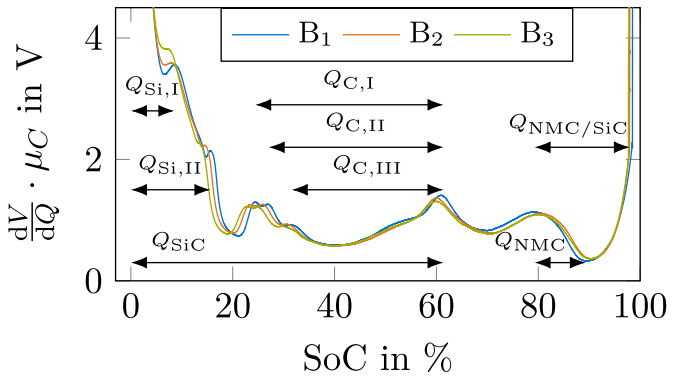

Fig. 4. Results of the DVA performed for the different batches. The shown DVA curve of B_1, B_2 and B_3 represent the averaged DVA of all single cell DVAs of the respective batch. Characteristic capacities are marked for B_1 according to Ref. [21].

Table 5
Quantitative and qualitative overview of characteristic capacities of the DVA for all batches (see Fig. 4).

Capacity	Order	B_1	B_2 vs. B_1	B_3 vs. B_1
$Q_{Si,I}$	$B_1 > B_2 > B_3$	0.31 Ah	−9.4%	−20.7%
$Q_{Si,II}$	$B_1 > B_2 > B_3$	0.56 Ah	−8.2%	−16.7%
Q_{SiC}	$B_1 > B_2 > B_3$	2.16 Ah	−2.6%	−4.2%
$Q_{C,I}$	$B_1 > B_3 > B_2$	1.30 Ah	−1.3%	−1.3%
$Q_{C,II}$	$B_3 > B_1 > B_2$	1.20 Ah	−0.7%	+0.2%
$Q_{C,III}$	$B_3 > B_1 > B_2$	1.04 Ah	−0.4%	+0.2%
Q_{NMC}	$B_1 > B_2 > B_3$	0.37 Ah	−5.2%	−5.8%
$Q_{NMC/SiC}$	$B_1 > B_2 > B_3$	0.69 Ah	−11.0%	−11.5%

① The first peak between 3.4 V and 3.5 V of the full cell voltage, results from the deintercalation of lithium out of the SiC anode.
② The following peak around 3.6 V occurs from the phase transition within the NMC cathode.
③/④ The smaller peak at around 3.9 V and the large peak around 4.1 V are very specific to NMC-811 cathodes.

Note that the assignments made are based on full cell voltages, which is why the corresponding voltages are slightly higher because of the performed half cell measurement against Li/Li^+ by Refs. [24,25]. Especially, peak ④ strongly correlates to the presence of nickel within the cathode material, which is why higher deflections can be seen as an indicator for increased nickel ratios [24–26]. Consequently, deviations in the height of the first and the last peak can be assigned to varying material compositions. Therefore, a higher first peak corresponds to an increased capacity of the anode and a higher last peak to a more nickel-rich cathode. Shifted peaks would indicate a change in electrode balancing. Comparing the DCA of the batches, two major facts can be observed. First, a shift around 10 mV of the first peak ① for B_1 can be recognized as compared to B_2 and B_3. Second, the peaks ① and ④ are more prominent for B_1 (1.4/3.1 Ah V^{-1}) as compared to B_2 (1.3/2.8 Ah V^{-1}) and B_3 (1.3/2.8 Ah V^{-1}). The complete measurement data of the DCA is illustrated in Fig. A.6 b).

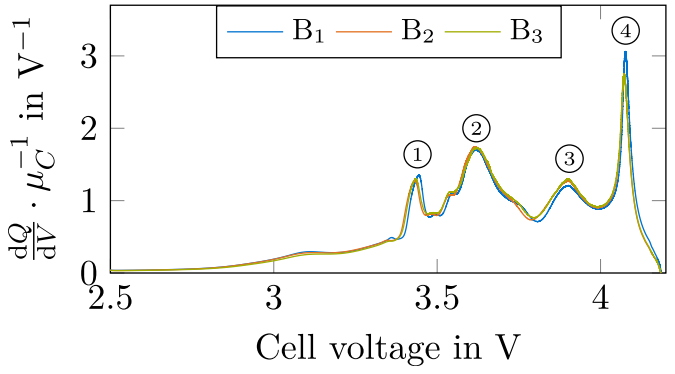

Fig. 5. Results of the DCA performed for the different batches. The shown DCA curve of B_1, B_2 and B_3 represent the averaged DCA of all single cell DCAs of the respective batch. Characteristic peaks are marked according to Refs. [24–26].

4. Discussion

The development of μ_C shows decreasing capacities with later production dates. Keeping in mind that the data sheet offers a minimum capacity of 3.35 Ah, a trend appears, suggesting that the manufacturer may have continuously optimized the production to economize material consumption and costs. If one correlates the development of capacity and energy density distribution of the different batches, this statement is clearly supported by the decreasing energy density of B_2 and B_3 as compared to B_1. Furthermore, κ_C increased over the production time, which could be assigned to a varying production quality. On the other hand, comparing these values with κ_C of other investigations (Table 1), it can be recognized that only established material combinations such as LFP or NCA show lower deviations. Since κ_C of the analyzed batches amounted to values of 0.4% and below, high production standards can be assumed, especially if these deviations are compared to studies dealing with NMC.

Regarding the impedance development of μ_R, the same trend can be observed as for the capacity. Therefore, μ_R decreased for B_2 and B_3 as compared to B_1. However, κ_R increased to a greater extent as compared to κ_C. This can be seen if one compares the factor between κ_C and κ_R for the different batches. B_1 and B_2 show a factor (κ_R/κ_C) of 3.4 and 2.8 between κ_R and κ_C, whereas the factor increases to 8.1 for B_3. The reason for the increased value of B_3 can be identified in Fig. 2, where two distinguished peaks are clearly visible for B_3. Within the distributions around the peaks, data is normally distributed. However, taking the complete distribution into account, the data is not normally distributed, which in turn provokes a higher σ_R for B_3. Nevertheless, normal distribution is used for statistic analysis due to comparative reasons, as it was equally done by Rumpf et al. [1]. Therefore, within the analyzed batches, κ_R showed the highest values for B_3 and was amounted to 3.4%. Comparing these values with the results of other studies, the relative deviation of B_3 is within the range of other κ_R ranging up to 5.7%. On the other hand, κ_R of B_1 falls below the lower border of 0.7% of existing studies. More important than comparing relative deviations, however, is what can be derived from the distributions of C and R_i. Hence, the assumption of An et al. [15] can be confirmed, namely that cell manufacturers sort according to capacity and not according to resistance.

With this knowledge, the battery pack manufacturers have to rethink their cell matching strategies depending on the interconnection of their system. For example, a pure serial connection of cells would benefit from equal capacities of the single cells, whereas a combined serial and parallel connection has also to take into account the differences in resistance to avoid higher imbalance currents [13,27]. Furthermore, low initial cell-to-cell variations do not have to mean low cell-to-cell variations after cycling [5,10,12,13,16,18]. Consequently, cell matching strategies during the assembling process of the battery pack can be ideally complemented with an intelligent system that uses strategies such as active balancing, by-passing or isolation to compensate cell-to-cell variations over time [28,29].

Finally, we consider possible reasons for the decreasing capacity and energy density from B_1 to B_2 and B_3. DVA and DCA are therefore used to identify possible changes of the active material between B_1, B_2, and B_3. Since the peaks for the varying batches have almost not

shifted within the DCA, uneven cell balancing cannot be given as the reason for the decreasing capacities. However, Fuchsbichler et al. [25] found that the height of peak ① correlates with the silicon content. Since the different batches show different heights in exactly this peak, this can be seen as an indicator to attribute the capacity change between the batches to changed silicon contents within the anode. This finding is supported by the development of the energy density illustrated in Fig. 3.

As the capacities of $Q_{C,I-III}$ also show a variation of at most 1.3% as compared to $Q_{Si,I-II}$ (max. 20.7%, see Table 5) for the different batches, the decreasing capacity is more likely evoked by a reduction of silicon within the anode rather than a reduced content of graphite. Additionally, the higher peak ④ within Fig. 5 indicates increased nickel ratios within the NMC cathode of B_1 and an adaptation of the NMC composition for B_2 and B_3 [24,26]. Furthermore, the capacities of Q_{SiC} and $Q_{NMC/SiC}$ depicted from the DVA (see Fig. 3 and Table 2) show the highest values for B_1, followed by B_2 and B_3. This in turn also indicates a decreased ratio of silicon within the graphite anode for B_2 and B_3 as compared to B_1. By combining the results of DVA and DCA, the decreased capacity of B_2 and B_3 as compared to B_1 can most likely be explained by a superposition of decreasing ratios of silicon within the graphite anode ($B_1 > B_2 > B_3$) and a lower nickel content within the NMC cathode [24] for B_2 and B_3 as compared to B_1. Fig. 3 illustrates the decreasing energy densities from B_1 to B_2 and B_3, which underlines these findings.

5. Conclusion

Cell-to-cell variation analysis was performed for three different batches of commercial LIBs. In total, 408 high-energy LIBs containing nickel-rich cathode active material and silicon-graphite anode active material were analyzed over a period of almost three years of the product life cycle. A sequence of measurement tests was presented to determine C and R_i parameter variations, which can be used for further studies to improve comparability. Additionally, strategies to reduce the test time, in case of limited time or resources, were discussed. Furthermore, the cell's OCV was measured for subsequent DVA and DCA to investigate differences in active material composition between the batches and to explain the development of cells' capacity and energy density.

The exact reasons for varying parameter variations are often difficult to determine with certainty, since imbalances within interconnected LIBs can be caused by both intrinsic and extrinsic reasons [9]. Thus, varying active material compositions (intrinsic) or fluctuating quality of their material components such as silicon or graphite (extrinsic) can be mentioned as underlying reasons for cell-to-cell variations. For the customer, these reasons are often neither accessible nor decisive. However, the effects of these changes on performance parameters such as capacity, resistance or cycle stability are crucial, as they are reflected in the system's performance. As a result of this study, it can be stated that changes between batches are likely to appear and should thus be considered by the customer. Consequently, customers should keep in mind that material composition can change and affect the system performance, even if no product changes were communicated by the cell manufacturer.

If one aims to compare cell-to-cell variations of different batches or material combinations, the relative coefficients of deviation κ_C and κ_R are important parameters to ensure comparability and to quantify the homogeneity within a batch. Therefore, it could be shown that the deviations of κ_C, especially for established cell chemistries such as LFP, are relatively small, whereas for novel material combinations, values are not yet available in the literature. Accordingly, the results of this study show that κ_C (and κ_R) can change from batch to batch, even if the values always remained within the range known from the literature or even fell below it. However, the increasing values of κ_C and κ_R over the analyzed period suggest that, for novel materials, it can last a few years until the cell manufacturer has found the optimum composition to achieve both a high energy density and cycle stability. Furthermore, the capacity could be detected as the decisive parameter for the cell matching process by the cell manufacturer. This is due to the fact that κ_C remained at a very low level compared to κ_R for both the analyzed batches and the deviations observed from the literature.

In addition, the potential of DVA and DCA to describe the differences between different batches was demonstrated. The major advantage of these methods is that they are non-destructive and therefore easily applicable to other studies. With the help of these methods, the measured voltage was used to directly access electrode characteristics. Researchers can therefore use the test procedure presented in Table 3 and perform DVA and DCA to compare their results with the presented samples in order to obtain indications for shifted cell balancing or modified electrode material compositions. A changed electrode balance is indicated by a shift in the curves of DVA and DCA, while a modified material composition can be recognized by varying peak heights. For the batches analyzed, DVA and DCA have shown that material composition has changed over the product life cycle and that the decreasing capacity is due to reduced silicon within the anode active material and not to a shifted cell balancing. The development of the energy density also supports the results found by the DVA and DCA, since a significant reduction could be measured. For scientists who are interested in the exact material composition of the electrode materials, the methods described provide indicators that can be verified by destructive methods such as mass spectroscopy.

Generally, it should be noted that the results obtained are based on commercially available cells and that lower cell-to-cell variations may apply to higher standards for industrial purposes. Based on the findings of this work, two main studies should be carried out in the future. First, the effects of varying material composition on the aging behavior has to be investigated. Second, the impact of cell-to-cell variations presented here on the performance of interconnected systems over lifetime should be analyzed by both simulation and measurement studies. Both studies are part of ongoing investigations and will be the subject of our future work.

CRediT authorship contribution statement

M. Schindler: Conceptualization, Methodology, Formal analysis, Investigation, Writing - original draft, Writing - review & editing. **J. Sturm:** Methodology, Investigation, Writing - review & editing. **S. Ludwig:** Investigation, Writing - review & editing. **J. Schmitt:** Investigation, Writing - review & editing. **A. Jossen:** Resources, Writing - review & editing.

Declaration of competing interest

The authors declare that they have no known competing financial interests or personal relationships that could have appeared to influence the work reported in this paper.

Acknowledgments

The results presented were achieved in association with an INI.TUM project, funded by the AUDI AG. Additionally, this work has received funding from the European Union's Horizon 2020 research and innovation programme under the grant 'Electric Vehicle Enhanced Range, Lifetime And Safety Through INGenious battery management' [EVERLASTING-713771]. The efforts of Axel Durdel and Lucas Koltermann at Technical University of Munich (TUM) are gratefully acknowledged.

Appendix A. Measurement data

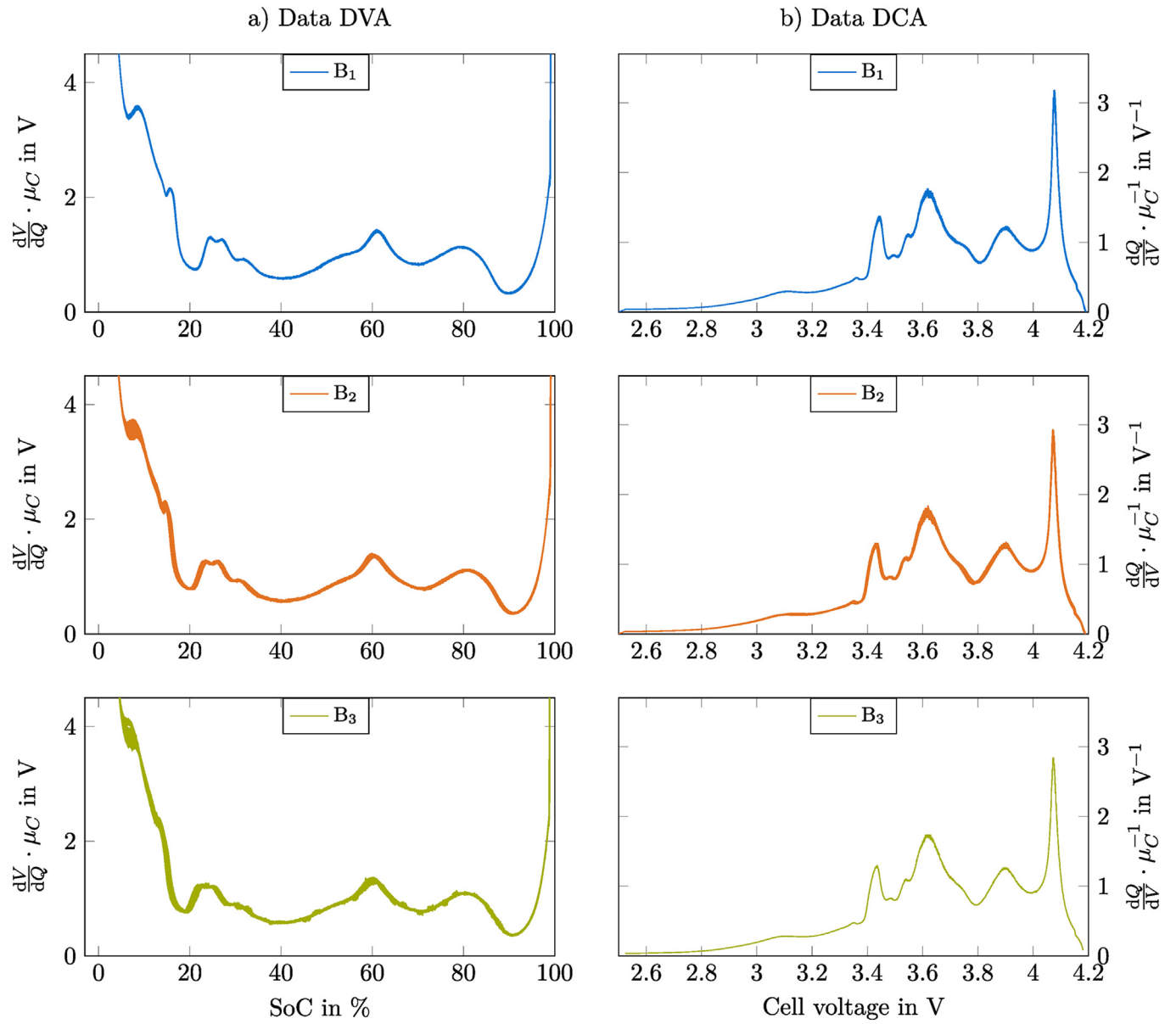

Fig. A.6. Summary of all measurement data for B_1, B_2 and B_3. Part a) shows the results of the DVA for the different batches. Part b) illustrates the results of the DCA.

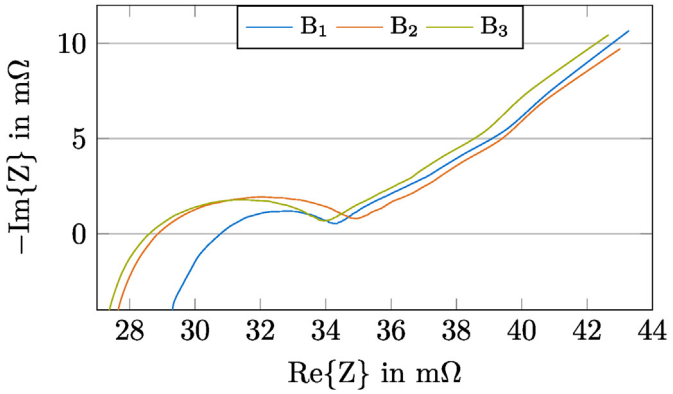

Fig. A.7. Results of the EIS measurement for a representative cell of B_1, B_2 and B_3.

Table A.6
Influence of the conditioning cycles on the difference between the capacity loss per cycle.

N_{FC}	B_1	B_2	B_3
1	–	–	–
2	12.1 mAh	11.3 mAh	12.0 mAh
3	3.74 mAh	3.76 mAh	4.97 mAh
4	1.45 mAh	0.37 mAh	0.16 mAh
5	1.59 mAh	0.01 mAh	1.36 mAh

Table A.7
Nomenclature

Greek symbols		
Symbol	Unit	Description
κ	%	relative coefficient of variation
μ	mWh kg^{-1}, Ah, mΩ	mean
σ	mWh kg^{-1}, mAh, mΩ	standard deviation
Latin symbols		
Symbol	Unit	Description
AC	A	alternating current
B		batch
C	Ah	capacity
CC	A	constant current
CV	A	constant voltage
CC-CV	A	constant current - constant voltage
DC	A	direct current
FC		full cycle
I	A	applied charge or discharge current
N_{FC}		number of full cycles
R_i	Ω	internal resistance
$t_{Ch\text{-}Dch}$	Ω	resting time between charge and discharge
Indices		
Symbol		Description
1−3		batch number
C		capacity
E		energy density
R		internal resistance

References

[1] Rumpf K, Naumann M, Jossen A. Experimental investigation of parametric cell-to-cell variation and correlation based on 1100 commercial lithium-ion cells. J Energy Storage 2017;14:224−43. https://doi.org/10.1016/j.est.2017.09.010. ISSN 2352152X.

[2] Rumpf K, Rheinfeld A, Schindler M, Keil J, Schua T, Jossen A. Influence of cell-to-cell variations on the inhomogeneity of lithium-ion battery modules. J Electrochem Soc 2018;(165):A2587−607. https://doi.org/10.1149/2.0111811jes.

[3] Chang L, Zhang C, Wang T, Yu Z, Cui N, Duan B, Wang C. Correlations of cell-to-cell parameter variations on current and state-of-charge distributions within parallel-connected lithium-ion cells. J Power Sources 2019;437:226869. https://doi.org/10.1016/j.jpowsour.2019.226869. ISSN 03787753.

[4] Feng F, Hu X, Hu L, Hu F, Li Y, Zhang L. Propagation mechanisms and diagnosis of parameter inconsistency within Li-Ion battery packs. Renew Sustain Energy Rev 2019;112(102−113). https://doi.org/10.1016/j.rser.2019.05.042. ISSN 13640321.

[5] Schuster SF, Brand MJ, Berg P, Gleissenberger M, Jossen A. Lithium-ion cell-to-cell variation during battery electric vehicle operation. J Power Sources 2015;297:242−51. https://doi.org/10.1016/j.jpowsour.2015.08.001. ISSN 03787753.

[6] Shin D, Poncino M, Macii E, Chang N. A statistical model of cell-to-cell variation in Li-ion batteries for system-level design. In: 2013 IEEE international symposium on low power electronics and design (ISLPED). Piscataway, NJ: IEEE; 2013, ISBN 978-1-4799-1235-3. p. 94−9. https://doi.org/10.1109/ISLPED.2013.6629273.

[7] Paul S, Diegelmann C, Kabza H, Tillmetz W. Analysis of ageing inhomogeneities in lithium-ion battery systems. J Power Sources 2013;239:642−50. https://doi.org/10.1016/j.jpowsour.2013.01.068. ISSN 03787753.

[8] Zheng Y, Han X, Lu L, Li J, Ouyang M. Lithium ion battery pack power fade fault identification based on Shannon entropy in electric vehicles. J Power Sources 2013;223:136−46. https://doi.org/10.1016/j.jpowsour.2012.09.015. ISSN 03787753.

[9] Dubarry M, Vuillaume N, Liaw BY. Origins and accommodation of cell variations in Li-ion battery pack modeling. Int J Energy Res 2010;34(2):216−31. https://doi.org/10.1002/er.1668. ISSN 0363907X.

[10] Devie A, Baure G, Dubarry M. Intrinsic variability in the degradation of a batch of commercial 18650 lithium-ion cells. Energies 2018;11(5):1031. https://doi.org/10.3390/en11051031.

[11] Dubarry M, Truchot C, Cugnet M, Liaw BY, Gering K, Sazhin S, Jamison D, Michelbacher C. Evaluation of commercial lithium-ion cells based on composite positive electrode for plug-in hybrid electric vehicle applications. Part I: initial characterizations. J Power Sources 2011;196(23):10328−35. https://doi.org/10.1016/j.jpowsour.2011.08.077. ISSN 03787753.

[12] Campestrini C, Keil P, Schuster SF, Jossen A. Ageing of lithium-ion battery modules with dissipative balancing compared with single-cell ageing. J. Energy Storage 2016;6:142−52. https://doi.org/10.1016/j.est.2016.03.004. ISSN 2352152X.

[13] Baumann M, Wildfeuer L, Rohr S, Lienkamp M. Parameter variations within Li-Ion battery packs − theoretical investigations and experimental quantification. J. Energy Storage 2018;18:295−307. https://doi.org/10.1016/j.est.2018.04.031. ISSN 2352152X.

[14] An F, Chen L, Huang J, Zhang J, Li P. Rate dependence of cell-to-cell variations of lithium-ion cells. Sci Rep 2016;6:35051. https://doi.org/10.1038/srep35051.

[15] An F, Huang J, Wang C, Li Z, Zhang J, Wang S, Li P. Cell sorting for parallel lithium-ion battery systems: evaluation based on an electric circuit model. J. Energy Storage 2016;6:195−203. https://doi.org/10.1016/j.est.2016.04.007. ISSN 2352152X.

[16] Rothgang S, Baumhofer T, Sauer DU. Diversion of aging of battery cells in automotive systems. In: 2014 IEEE vehicle power and propulsion conference (VPPC). Piscataway, NJ: IEEE; 2014, ISBN 978-1-4799-6783-4. p. 1−6. https://doi.org/10.1109/VPPC.2014.7007050.

[17] Barreras JV, Raj T, Howey DA, Schaltz E. Results of screening over 200 pristine lithium-ion cells. In: IEEE vehicle power and propulsion conference. Belfort: VPPC); 2017. p. 1−6. https://doi.org/10.1109/VPPC.2017.8331060.

[18] Baumhöfer T, Brühl M, Rothgang S, Sauer DU. Production caused variation in capacity aging trend and correlation to initial cell performance. J Power Sources 2014;247:332−8. https://doi.org/10.1016/j.jpowsour.2013.08.108. ISSN 03787753.

[19] Zou H, Zhan H, Zheng Z. A multi - factor weight Analysis method of lithiumion batteries based on module topology. In: International conference on Sensing,Diagnostics, prognostics, and control (SDPC). IEEE; 2018, ISBN 978-1-5386-6057-7. p. 61−6. https://doi.org/10.1109/SDPC.2018.8664989. 8/15/2018 - 8/17/2018.

[20] Barai A, Uddin K, Widanage WD, McGordon A, Jennings P. A study of the influence of measurement timescale on internal resistance characterisation methodologies for lithium-ion cells. Sci Rep 2018;8(1):21. https://doi.org/10.1038/s41598-017-18424-5.

[21] Zilberman I, Sturm J, Jossen A. Reversible self-discharge and calendar aging of 18650 nickel-rich, silicon-graphite lithium-ion cells. J Power Sources 2019;425:217−26. https://doi.org/10.1016/j.jpowsour.2019.03.109. ISSN 03787753.

[22] Zilberman I, Ludwig S, Jossen A. Cell-to-cell variation of calendar aging and reversible self-discharge in 18650 nickel-rich, silicon−graphite lithium-ion cells. J. Energy Storage 2019;26:100900. https://doi.org/10.1016/j.est.2019.100900. ISSN 2352152X.

[23] Gyenes B, Stevens DA, Chevrier VL, Dahn JR. Understanding anomalous behavior in coulombic efficiency measurements on Li-ion batteries. J Electrochem Soc 2015;162(3):A278−83. https://doi.org/10.1149/2.0191503jes. ISSN 0013-4651.

[24] Jung R, Metzger M, Maglia F, Stinner C, Gasteiger HA. Oxygen release and its effect on the cycling stability of $LiNi_xMn_yCo_zO_2$ (NMC) cathode materials for Li-ion batteries. J Electrochem Soc 2017;164(7):A1361−77. https://doi.org/10.1149/2.0021707jes. ISSN 0013-4651.

[25] Fuchsbichler B, Stangl C, Kren H, Uhlig F, Koller S. High capacity graphite−silicon composite anode material for lithium-ion batteries. J Power Sources 2011;196(5):2889−92. https://doi.org/10.1016/j.jpowsour.2010.10.081. ISSN 03787753.

[26] Noh H-J, Youn S, Yoon CS, Sun Y-K. Comparison of the structural and electrochemical properties of layered $Li[Ni_xMn_yCo_z]O_2$ (x = 1/3, 0.5, 0.6, 0.7, 0.8 and 0.85) cathode material for lithium-ion batteries. J Power Sources 2013;233:121−30. https://doi.org/10.1016/j.jpowsour.2013.01.063. ISSN 03787753.

[27] Brand MJ, Hofmann MH, Steinhardt M, Schuster SF, Jossen A. Current distribution within parallel-connected battery cells. J Power Sources 2016;334:202−12. https://doi.org/10.1016/j.jpowsour.2016.10.010. ISSN 03787753.

[28] Barreras JV, Pinto C, de Castro R, Schaltz E, Andreasen SJ, Araujo RE. Multi-objective control of balancing systems for Li-ion battery packs: a paradigm shift?. In: 2014 IEEE vehicle power and propulsion conference (VPPC). Piscataway, NJ: IEEE; 2014. p. 1−7. https://doi.org/10.1109/VPPC.2014.7007107. 978-1-4799-6783-4.

[29] Zilberman I, Ludwig S, Schiller M, Jossen A. Online aging determination in lithium-ion battery module with forced temperature gradient. J. Energy Storage 2020;28:101170. https://doi.org/10.1016/j.est.2019.101170. ISSN 2352152X.